Multiple Ionization Bursts in Laser-Driven Hydrogen Molecular Ion

Norio Takemoto and Andreas Becker

JILA and Department of Physics, University of Colorado, 440 UCB, Boulder, Colorado 80309-0440, USA

(Received 14 June 2010; published 12 November 2010)

Theoretical study on H_2^+ in an intense infrared laser field on the attosecond time scale reveals that the molecular ion shows multiple bursts of ionization within a half-cycle of the laser field oscillation, in contrast to the widely accepted tunnel ionization picture for an atom. These bursts are found to be induced by transient localization of the electron at one of the nuclei, and a relation between the time instants of the localization and the vector potential of the laser light is derived. A scheme is proposed to probe the localization dynamics by an extreme ultraviolet laser pulse.

DOI: 10.1103/PhysRevLett.105.203004 PACS numbers: 32.80.Rm, 33.80.Rv

Many phenomena induced by the intense laser-matter interaction are known to be initiated by the release of an electron from the parent atom or molecule [1], which is often understood in terms of the quasistatic tunnel ionization picture. According to this picture, the electron tunnels through the barrier created by the binding potential of the ionic core and the electric potential of the laser field. Thus, in the oscillating electric field of laser light, the electron is expected to escape most likely at the peak of the electric field strength in every half-cycle as the barrier becomes the thinnest. This expectation is in agreement with the time dependence of the ionization rate for an atom predicted by the well-known tunnel formula [2,3] and shown in Fig. 1(a), which was also supported in a recent experiment [4]. However, our theoretical results show that molecules can exhibit not only one but multiple bursts of ionization within a half-cycle of the laser field. For example, the ionization rate of H_2^+ shown in Fig. 1(b) has two maxima within a half-cycle and minima near the peaks of the laser electric field.

In this Letter we show that these multiple ionization bursts (MIBs) are related to transient electron localization (EL) at one of the protons on the attosecond time scale. The localization is due to the strong coupling between a pair of states with opposite parities, called the charge-resonant (CR) states [5], which leads to more complex electron dynamics in a molecule than in an atom, as it has been reported before [6,7]. Despite the complexity of the electron dynamics, we derive a simple relation of the instants of EL to the vector potential of the laser field and the coupling strength between the CR states. This enables us to generalize our observations for the simplest molecule and to predict a similar modification of the tunnel ionization picture for other molecules having the CR states as well. To probe the transient EL in experiments, we propose a method to retrieve the laser-dressed quantum state of H_2^+ from an interference pattern in the photoelectron momentum distribution generated by applying an attosecond extreme ultraviolet (XUV) pulse.

For the present analysis we have solved the time-dependent Schrödinger equation (TDSE) for a model of H_2^+ in which the electronic and nuclear motions are restricted along the polarization direction of the linearly polarized laser pulse. The Hamiltonian of this system is given by (Hartree atomic units are used throughout) [8]:

$$H(t) = -\frac{1}{2\mu_R}\frac{\partial^2}{\partial R^2} - \frac{1}{2\mu_z}\frac{\partial^2}{\partial z^2} - \frac{1}{\sqrt{(z-\frac{R}{2})^2 + a_e}} - \frac{1}{\sqrt{(z+\frac{R}{2})^2 + a_e}} + \frac{1}{\sqrt{R^2 + a_n}} + \beta z E(t), \quad (1)$$

where R is the internuclear distance, z is the position of the electron measured from the center-of-mass of the protons, $\mu_R = M/2$ and $\mu_z = 2M/(2M+1)$ are the reduced masses with $M = 1.836 \times 10^3$ a.u. being the proton mass, $a_e = 1.0$ a.u. and $a_n = 0.03$ a.u. are the soft-core parameters [9], $\beta = 1 + 1/(2M+1)$, and $E(t)$ is the laser electric field. It has been shown before that this type of reduced-dimensional models reproduce experimental results at least qualitatively [9–11]. The ionization rate in Fig. 1(b) was calculated as the out-going probability flux from the rectangular domain, -8.4 a.u. $< z < 8.4$ a.u. and

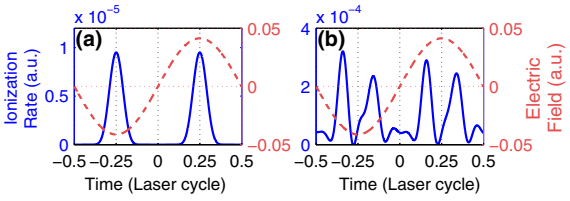

FIG. 1 (color online). Time-dependent ionization rates (solid blue curves) of (a) H atom [2] and (b) H_2^+ molecular ion over a single period at the peak of a laser pulse, represented by its electric field (dashed red curves). The ionization rate of H_2^+ is for the range of internuclear distance, 6.75 a.u. $< R <$ 7.25 a.u., and was obtained by numerical simulation of TDSE. Pulse parameters in the calculations were wavelength: 800 nm, peak intensity: 6×10^{13} W/cm^2, pulse duration: 26.69 fs (FWHM).

6.75 a.u. $< R <$ 7.25 a.u., toward $|z| \to \infty$ normalized by the probability inside this domain, under a laser pulse with the wavelength of 800 nm, peak intensity 6×10^{13} W/cm^2, and FWHM duration 26.69 fs.

We present in Fig. 2(a) how the electron density evolves in time under the same laser pulse and in the same scope of R as used in Fig. 1(b). This result shows that the electron density bound to the protons at around $z \approx \pm 3.5$ a.u. is released in several bunches within a half-cycle of the laser field, consistently with the observation in Fig. 1(b). In the following, we trace the origin of these MIBs in the time evolution of the electron density by simplifying the model.

Figure 2(b) shows the electron density calculated by fixing the nuclear positions at $R = 7$ a.u. and letting $M \to \infty$. This fixed-nuclei model reproduces the result of the moving-nuclei model in Fig. 2(a) almost perfectly, indicating that the coupling between the electronic and nuclear motions is not essential for the formation of the MIBs. In Fig. 2(c), in the fixed-nuclei model, we absorbed the ionizing wave packets soon after they left the protons by using a $\cos^{1/2}$-mask function set over 6.6 a.u. $< |z| <$ 11 a.u. This result shows that the bound electron density is transiently localized at one of the two protons at the same instants as the ionization bursts marked by the circles in panel (b). Part of the wave packets released in the bursts during the time period in which $|E(t)|$ is decreasing ($-0.25 < t < 0$ and $0.25 < t < 0.5$ laser cycles in Fig. 2) can return to the protons [1,12]. Such rescattering wave packets create the modulation of the density including the enhancements at the cross marks in Fig. 2(b) due to the interference with the bound wave packet and also the finer fringes in the ionizing density at $|z| \gtrsim 8$ a.u. due to the interference with the wave packets just released from the protons.

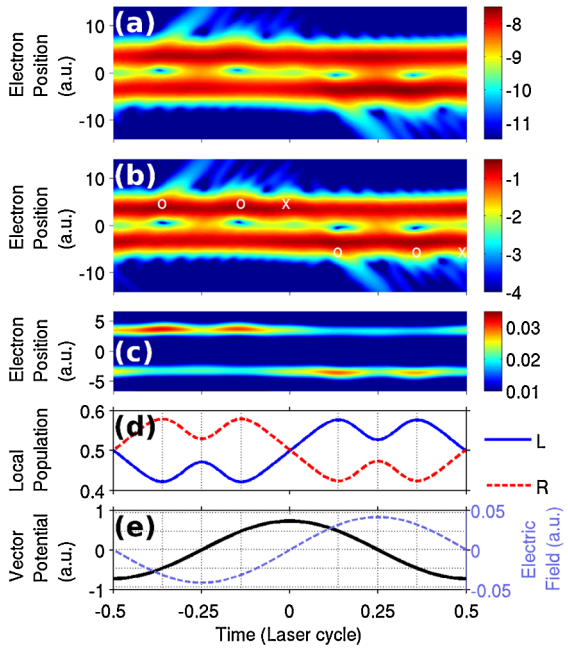

FIG. 2 (color online). Electron density (a) integrated over 6.75 a.u. $< R <$ 7.25 a.u. in the moving-nuclei model and (b) in the fixed-nuclei model at $R = 7$ a.u. as a function of time and electron position (shown on a $\log_{10}$ scale). (c) Electron density in the fixed-nuclei model with absorber near the nuclei. (d) Electron populations in the localized states, $|L\rangle$ and $|R\rangle$, in the two-state model. (e) Vector potential (solid line) and electric field (dashed line) of the laser light. Horizontal and vertical grid lines represent $A(t_{\rm loc})$ and $t_{\rm loc}$, respectively.

From the analysis so far, we can conclude that the MIBs are induced by the transient EL at one of the protons while the (rescattering) dynamics of the electronic wave packets in the continuum does not affect the time instants of the MIBs. This also substantiates that the present 1D models are sufficient for the analysis since effects of spreading in the transverse direction are negligible for the bound wave packets. In previous theoretical results, the laser-driven electron dynamics *inside* the molecule has been recognized to be complex and sometimes counterintuitive [6], and, in particular, the existence of the sub-laser-cycle EL has been pointed out [7]. The present work elucidates that this ultrafast EL also makes the ionization dynamics of H_2^+ qualitatively different from that of atoms and may give rise to a paradigm shift from the widely accepted tunnel ionization picture.

In order to further analyze the phenomenon of MIBs, we investigate the bound state dynamics using a simple model which incorporates only the ground ($|g\rangle$) and first-excited ($|u\rangle$) electronic states of H_2^+. These two states can be written as superpositions, $|g\rangle = [|L\rangle + |R\rangle]/\sqrt{2}$ and $|u\rangle = [|L\rangle - |R\rangle]/\sqrt{2}$, of the ground states of H atom, $|L\rangle$ and $|R\rangle$, centered at the protons at $z = -R/2$ and $z = R/2$, respectively. During the interaction with laser light, the eigenstates $|g\rangle$ and $|u\rangle$ mix, and the electron is driven between the two protons. This generates a large transition dipole $d_{gu} = -\langle g|z|u\rangle$, which is proportional to R at large R, and is known as the CR mechanism [5,9,13]. The two-state model is applicable to the present case since at $R = 7$ a.u. the $|g\rangle$ and $|u\rangle$ states are almost degenerate and well isolated from the higher-lying excited electronic states on the scale of the infrared (IR) photon energy. The time evolution of the state $|\Psi(t)\rangle$ of this model in a laser field can be described in the basis of Floquet states [14–16]. Using a series expansion for the Floquet states [16], we obtained expressions for the local populations at the respective protons, $|\langle L|\Psi(t)\rangle|^2$ and $|\langle R|\Psi(t)\rangle|^2$. From the condition $d[|\langle L|\Psi(t)\rangle|^2]/dt = 0$, we derive that population at one of the protons is maximized at the instants $t_{\rm loc}$ at which the vector potential satisfies

$$A(t_{\rm loc}) = A_0 \sin(\omega t_{\rm loc} + \varphi) = \frac{m\pi + \chi}{2d_{gu}}, \qquad (2)$$

where $m = 0, \pm 1, \pm 2, \ldots$, and χ is a mixing angle determined by the quantum amplitudes c_1 and c_2 of the Floquet states which reduces to $|g\rangle$ and $|u\rangle$ at zero laser intensity, respectively, with $\cos\chi = (|c_1|^2 - |c_2|^2)/C$, $\sin\chi = 2\mathrm{Im}[c_1^* c_2]/C$, and $C = \sqrt{(|c_1|^2 - |c_2|^2)^2 + 4(\mathrm{Im}[c_1^* c_2])^2}$.

Furthermore, from the sign of $d^2|\langle L|\Psi(t_{\rm loc})\rangle|^2/dt^2$, we can predict that the electron density is localized at the proton down the slope of the electric potential of the laser field at those $t_{\rm loc}$ corresponding to odd m. Previously, the EL was analyzed in terms of the phase-adiabatic states, but numerical computation was necessary to predict the instants of the maximum localization [7]. In Fig. 2(d), the local populations, $|\langle L|\Psi(t)\rangle|^2$ and $|\langle R|\Psi(t)\rangle|^2$, calculated by the two-state model are plotted as a function of time. Comparison with the numerical results in Fig. 2(c) shows that time instants of the subcycle ionization bursts can be traced back to the simple condition (2).

We may emphasize that the *strong* and *exclusive* coupling between a pair of states, and hence the trapping of the population within such a pair, are the essence of the counterintuitive two-state dynamics inducing the MIBs. Thus, the current analysis applies in general to molecules in which the ground state is strongly coupled to one particular excited state, and to laser wavelengths which do not coincide with a resonant transition to any other state. In atoms, the first-excited state is coupled not only to the ground state but also with higher-lying excited states. Therefore, the EL cannot be induced, and MIBs have not been observed. Even in H_2^+, at around the equilibrium internuclear distance ($R_{\rm eq} \approx 2$ a.u.), the energy levels of $|g\rangle$ and $|u\rangle$ are not well isolated from the other states, and the transition dipole is not exclusive between these two states [5,9,13]. Therefore, the ionization dynamics becomes similar to atoms, and the standard quasistatic tunnel ionization picture should be recovered. On the other hand, in H_2^+ at larger R, where the coupling strength $d_{gu} \sim R/2$ becomes large, the electron density can be localized more than twice within a half-cycle at rather moderate laser intensity. Note that the coupling between CR states can be large and exclusive already at the equilibrium structure in other molecules [17].

As shown above, MIBs are caused by the localization of the electron at one of the protons. Previously, theoretical studies have shown that the time-evolving asymmetry of the electron density inside H_2^+ can be probed by an attosecond XUV pulse via the asymmetry of the photoelectron yield and momentum in opposite directions along the XUV laser polarization parallel to the molecular axis [18,19]. We propose here to extend this scheme by setting the polarization of the XUV pulse at an angle to the molecular axis and the polarization of the IR driving pulse and by analyzing the 2D photoelectron momentum distribution. As we will show below, this potentially enables us to *reconstruct* the temporal evolution of the *amplitudes* $c_L(t)$ and $c_R(t)$ of the two quantum states $|L\rangle$ and $|R\rangle$ composing the laser-dressed state of H_2^+.

To this end, we model the photoionization process due to the XUV pulse as a one-photon transition from the IR-laser-dressed bound state, $|\Psi(t)\rangle = c_L(t)|L\rangle + c_R(t)|R\rangle$, to the Volkov state of drift momentum $\mathbf{k}$ in the IR laser field. For simplicity, we assume here that the XUV pulse is polarized perpendicular to the molecular axis and its electric field has a Gaussian envelope as $\mathbf{E}_{\rm XUV}(t) = \hat{\boldsymbol{\epsilon}}_{\rm XUV} E^0_{\rm XUV} \exp[-(t-t_0)^2/\tau^2_{\rm XUV}]\cos(\Omega t + \varphi_{\rm XUV})$. At the limit of $\tau_{\rm XUV} \ll T_{\rm IR}$, where $\tau_{\rm XUV}$ is the pulse duration of the XUV pulse and $T_{\rm IR}$ is the period of the IR driving pulse, by applying Laplace's method of asymptotic analysis for the S-matrix element, we obtained the photoelectron momentum distribution as

$$
\begin{aligned}
|S_{fi}(\mathbf{k}, t_0)|^2 \sim{}& \pi^3 [E^0_{\rm XUV}]^2 \tau^2_{\rm XUV} |\tilde{d}_{\rm atom}(\mathbf{q}(t_0))|^2 \\
&\times \exp\left\{ -\frac{\tau^2_{\rm XUV}}{2}\left[\frac{|\mathbf{q}(t_0)|^2}{2} - \frac{E_g + E_u}{2} - \Omega \right]^2 \right\} \\
&\times \{ |c_L(t_0)|^2 + |c_R(t_0)|^2 + 2{\rm Re}[c_L(t_0) c^*_R(t_0)] \\
&\times \cos[\mathbf{q}(t_0)\cdot\mathbf{R}] - 2{\rm Im}[c_L(t_0) c^*_R(t_0)] \\
&\times \sin[\mathbf{q}(t_0)\cdot\mathbf{R}] \},
\end{aligned} \tag{3}
$$

where $\mathbf{q}(t_0) = \mathbf{k} + \mathbf{A}(t_0)$ is the photoelectron momentum $\mathbf{k}$ offset by the vector potential $\mathbf{A}(t_0)$ of the IR field at the peak t_0 of the XUV pulse, E_g and E_u are the energies of $|g\rangle$ and $|u\rangle$, respectively, and $\tilde{d}_{\rm atom}(\mathbf{q}) = \langle e^{i\mathbf{q}\cdot\mathbf{r}} | \hat{\boldsymbol{\epsilon}}_{\rm XUV} \cdot \mathbf{r} | \phi_{1s}(\mathbf{r})\rangle$ is the transition dipole between H atom 1s state to the plane wave state.

By fitting the model Eq. (3) to an experimentally obtained photoelectron momentum distribution, the quantum amplitudes $\{c_L(t_0), c_R(t_0)\}$ at the peak of the XUV probe pulse can be retrieved. In order to demonstrate the accuracy of this retrieval procedure, we simulated momentum distributions by solving the TDSE for a 2D model of H_2^+ with the internuclear distance fixed at $R = 7$ a.u. To fulfill the condition $\tau_{\rm XUV} \ll T_{\rm IR}$, we used an IR laser pulse with wavelength of 1400 nm, peak intensity 1.5×10^{13} W/cm^2, and FWHM pulse duration 14.01 fs. For the XUV laser field, the peak intensity was set at 1.0×10^{12} W/cm^2, wavelength at 25 nm, and FWHM at 500.3 as. By changing the delay Δt from the peak of the IR pulse to that of XUV pulse, photoelectron momentum distributions were calculated. Then, from these distributions, the background momentum distribution calculated by applying only the IR laser pulse was subtracted.

Figure 3 shows the XUV photoionization signal obtained by the numerical simulations at six delay times from $\Delta t = 0$ to 0.25 IR laser cycles. As the Gaussian factor in the model formula (3) suggests, the photoelectron momentum is distributed around the energy-conservation circle of radius $\sqrt{2[(E_g + E_u)/2 + \Omega]}$, whose center is streaked by the vector potential of the IR laser field as $\mathbf{k} = -\mathbf{A}(t_0)$ [20]. This ring distribution is multiplied by the atomic p_y-wave factor due to $|\tilde{d}_{\rm atom}|^2$, as well as the two-center interference pattern from which the ultrafast evolution of $c_L(t_0)$ and $c_R(t_0)$ can be retrieved.

In actual experiments, it is, however, difficult to determine the absolute value of the photoelectron momentum distribution. Under this restriction, the information about the common scale of $|c_L(t_0)|$ and $|c_R(t_0)|$ is lost, but we can

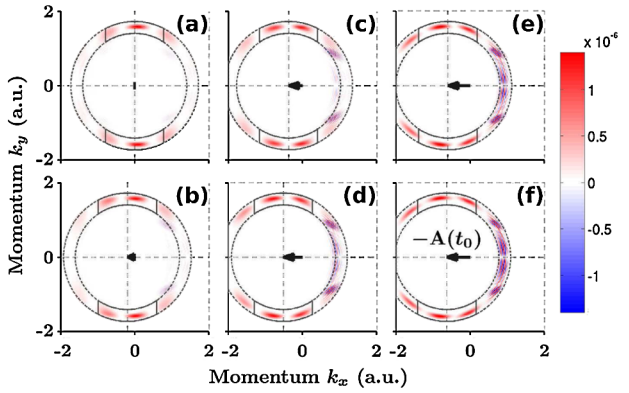

FIG. 3 (color online). XUV photoelectron signals at the XUV-IR delays of (a) $\Delta t = 0.00$, (b) $\Delta t = 0.05$, (c) $\Delta t = 0.10$, (d) $\Delta t = 0.15$, (e) $\Delta t = 0.20$, and (f) $\Delta t = 0.25$ IR cycles. ($\mathbf{R} \parallel \hat{x}$ and $\hat{\boldsymbol{\epsilon}}_{\mathrm{XUV}} \parallel \hat{y}$).

still retrieve the normalized populations, $P_L = |c_L|^2/(|c_L|^2 + |c_R|^2)$ and $P_R = |c_R|^2/(|c_L|^2 + |c_R|^2)$, as well as the relative phase $\alpha_{LR} = \arg[c_L c_R^*]$. Figure 4 shows these quantities retrieved from the distributions in Fig. 3 (and those at other XUV-IR delays). We also computed the exact time evolution of P_L, P_R, and α_{LR} in the TDSE simulation with only the IR pulse applied, and show the results in Fig. 4 by gray lines as reference. The comparison shows that the present method allows one to reconstruct the attosecond time evolution of the laser-dressed quantum state in H_2^+. We may note that due to the present assumption that the polarization direction of the XUV pulse is perpendicular to the molecular axis we obtain the same momentum distribution when P_L is exchanged with P_R. An extension to other alignment angles is straightforward, and in this case the set of values $\{P_L, P_R, \alpha_{LR}\}$ can be retrieved uniquely.

In summary, we have found that there can be MIBs from H_2^+ and other molecules with CR states within a half-cycle of the laser field oscillation in contrast to the widely accepted tunnel ionization picture. These bursts were shown to be induced by the transient EL inside the molecule on the attosecond time scale, and a simple expression to predict the number and instants of the EL was presented. Time evolution of the quantum state exhibiting such a localization behavior can be reconstructed in an experiment with an attosecond XUV pulse. Thus, the present results show how an analysis of the laser-driven quantum electron dynamics in molecules based on the recently advanced attosecond technology can provide new insights into a seemingly well-understood phenomenon.

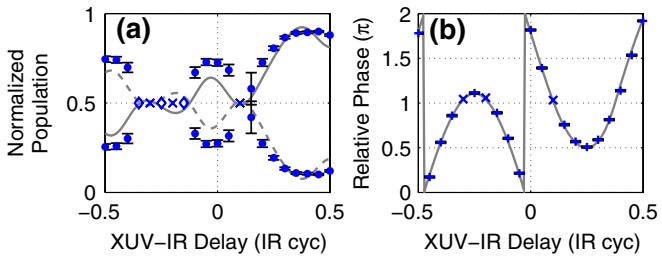

FIG. 4 (color online). (a) Normalized local populations P_L and P_R and (b) relative phase α_{LR} retrieved by the fitting procedure (markers) in comparison with the values obtained from the TDSE solutions (gray lines).

Beyond the paradigm shift from the tunnel ionization picture, our findings also suggest that in high harmonic generation, where the intermediate cation is actually dressed by the intense driving field, the ultrafast time evolution of the electronic state can be drastically different from that under the field-free condition if the cation is in a CR state. This should influence the results of molecular orbital tomography technique [21]. The MIBs also offer a control knob of the attosecond pulse generation for which the harmonics at the cutoff of the spectrum is used. The high harmonic photon energy corresponds to the kinetic energy of the electron acquired in the driving field, which is determined by the phase of the field at which the electron is released [1,12]. Our findings suggest that the ionization probability at a particular phase, and hence the harmonic efficiency at the cutoff, can be controlled.

We thank Professor H. Kono, Dr. F. He, Dr. C. Ruiz Méndez, and Dr. T. Popmintchev for helpful discussions. This work was partially supported by NSF.

[1] P. B. Corkum, Phys. Rev. Lett. **71**, 1994 (1993).
[2] L. D. Landau and E. M. Lifshitz, *Quantum Mechanics: Non-Relativistic Theory* (Elsevier, New York, 1977), 3rd ed.
[3] G. L. Yudin and M. Yu. Ivanov, Phys. Rev. A **64**, 013409 (2001).
[4] M. Uiberacker *et al.*, Nature (London) **446**, 627 (2007).
[5] R. S. Mulliken, J. Chem. Phys. **7**, 20 (1939).
[6] F. He, A. Becker, and U. Thumm, Phys. Rev. Lett. **101**, 213002 (2008).
[7] I. Kawata, H. Kono, and Y. Fujimura, J. Chem. Phys. **110**, 11 152 (1999).
[8] J. R. Hiskes, Phys. Rev. **122**, 1207 (1961).
[9] K. C. Kulander, F. H. Mies, and K. J. Schafer, Phys. Rev. A **53**, 2562 (1996).
[10] W. Qu *et al.*, Phys. Rev. A **65**, 013402 (2001).
[11] G. L. Ver Steeg, K. Bartschat, and I. Bray, J. Phys. B **36**, 3325 (2003).
[12] M. Lewenstein *et al.*, Phys. Rev. A **49**, 2117 (1994).
[13] R. Herman and R. F. Wallis, Astrophys. J. **123**, 353 (1956).
[14] F. Grossmann *et al.*, Phys. Rev. Lett. **67**, 516 (1991).
[15] M. Yu. Ivanov, P. B. Corkum, and P. Dietrich, Laser Phys. **3**, 375 (1993).
[16] A. Santana, J. M. Gomez Llorente, and V. Delgado, J. Phys. B **34**, 2371 (2001).
[17] L. Pauling, Proc. Natl. Acad. Sci. U.S.A. **25**, 577 (1939).
[18] G. L. Yudin *et al.*, Phys. Rev. A **72**, 051401(R) (2005).
[19] S. Gräfe, V. Engel, and M. Yu. Ivanov, Phys. Rev. Lett. **101**, 103001 (2008).
[20] J. Itatani *et al.*, Phys. Rev. Lett. **88**, 173903 (2002).
[21] J. Itatani *et al.*, Nature (London) **432**, 867 (2004).